Structural Regulation and Optical Properties of One-Dimensional ZnO Nanomaterials in Situ Grown from and on Brass Substrates

Xuebin Wang,[†] Kaifu Huo,[†,‡,§] Fan Zhang,[†] Zheng Hu,*[,†] Paul K. Chu,[§] Haisheng Tao,[†] Qiang Wu,[†] Yemin Hu,[†] and Jianmin Zhu[†]

Key Laboratory of Mesoscopic Chemistry of MOE and Jiangsu Provincial Laboratory for Nanotechnology, School of Chemistry and Chemical Engineering, National Laboratory of Solid State Microstructures, Nanjing University, Nanjing 210093, China, Hubei Province Key Laboratory of Ceramics and Refractories, College of Materials and Metallurgy, Wuhan University of Science and Technology, Wuhan 430081, China, and Department of Physics and Materials Science, City University of Hong Kong, Tat Chee Avenue, Kowloon, Hong Kong, China

Received: October 1, 2008; Revised Manuscript Received: October 31, 2008

One-dimensional ZnO nanostructures have been in situ grown on the conductive brass substrate by directly heating the $Cu_{0.70}Zn_{0.30}$ alloy foils in O_2/Ar at 550−900 °C. The growth process and products have been well characterized by means of X-ray diffraction, Raman scattering, electron microscopy, X-ray photoelectron, and photoluminescence spectroscopy. The results indicate that more Zn species is lost from the brass foils at the higher temperatures. Zn species is exhausted, and a sharp diffraction peak shift appears around 750 °C due to the quick depletion. The structures of the ZnO products have been systematically regulated and the more oxygen vacancy is associated with the higher reaction temperature. The correlation in between the oxygen vacancy concentration and the green and exciton emission for these products has been experimentally demonstrated and well understood, which is important for luminescence applications.

Introduction

Zinc oxide, a direct wide band gap (3.37 eV) semiconductor with a large exciton binding energy (60 meV), is one of the most important semiconductor materials given its unique properties and wide potential applications.[1] In the past few years, one-dimensional (1-D) ZnO nanostructures are particularly attractive and have become the focus of intensive research.[2] On the basis of these novel materials, some advanced optoelectronic and nanoelectronic devices such as nanolasers,[3] nanogenerators,[4] and various chemical and biological nanosensors[5] have been successfully demonstrated. To date, different preparation methods have been developed, various 1-D ZnO nanostructures synthesized,[6] and exciting properties disclosed.[7] As known, the application of nanomaterials depends not only on their properties but also on their junction with other elements of a system. Very recently, a convenient method for the direct and large-area growth of 1-D ZnO nanostructures on a conductive brass substrate has been developed in our group,[8] consisting of thermal oxidation of a $Cu_{0.66}Zn_{0.34}$ alloy foil in the presence of oxygen. Various 1-D nanostructures such as nanowires, nanobelts, nanocombs, and nanosheets have been in situ grown on the brass substrate under different reaction temperatures. Since the alloy foil functions as both Zn source and substrate for the growth of 1-D ZnO nanostructures; thus, the synthesis and assembly of ZnO nanostructures on a metallic substrate is accomplished in one step, and the naturally good adhesion or electrical connection between the ZnO nanostructures and the conductive substrate has been realized. Such a configuration of the product showed quite good field emission property, indicating the scientific interest and potential technological importance. In this work, the growth process has been further revealed and the structural regulation on the ZnO_{1-x} products with different oxygen vacancy (V_O) concentrations has been realized. The correlation among green emission, exciton emission, and oxygen vacancy concentration for these products has been experimentally demonstrated and well understood, which is important for luminescence applications.

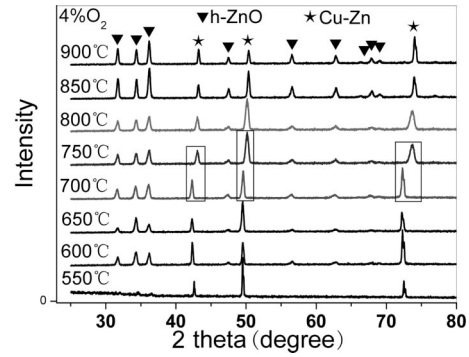

Figure 1. Room-temperature XRD patterns of the products obtained after annealing the $Cu_{0.70}Zn_{0.30}$ brass at different temperature.

Experimental Section

1-D ZnO nanostructures in situ grew from and on brass substrate by the same thermal oxidation process as described in detail in our previous paper.[8a] Briefly, commercial brass foil ($Cu_{0.70}Zn_{0.30}$, 8 × 8 mm^2) was polished with SiC sandpaper and then ultrasonically cleaned with acetone, ethanol, and deionized water sequentially. After dried in air, the brass foil was loaded on a ceramic substrate located in the center of a corundum tube inside a horizontal tube furnace. The reaction system was flushed

* To whom correspondence should be addressed. Phone: 0086-25-83686015. Fax: 0086-25-83686251. E-mail: zhenghu@nju.edu.cn.
† Nanjing University.
‡ Wuhan University of Science and Technology.
§ City University of Hong Kong.

10.1021/jp808679q CCC: $40.75
Published on Web 12/09/2008

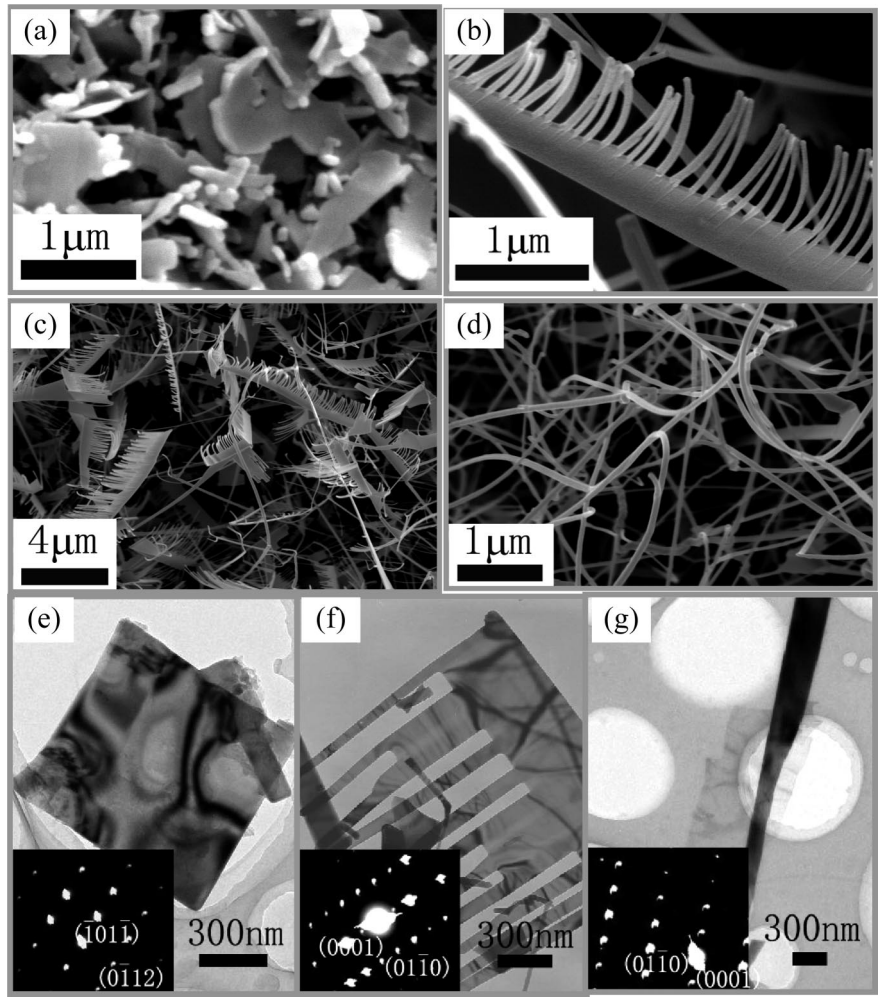

Figure 2. Typical SEM (a−d) and TEM (e−g) images and corresponding ED (insets) patterns of the products grown from and on Cu−Zn substrate at different T_R. (a) 550, (b, c) 600, (d) 650, (e) 550, (f) 600, and (g) 650 °C.

with Ar and heated to the designed temperature, and then O_2/Ar mixture with a flow rate of 50 sccm was introduced into the tube as the reagent gas. The system was maintained in the pressure of 100−150 Pa by a mechanical pump. After 60 min of reaction, the system was cooled down to room temperature in Ar, and a homogeneous white layer was formed on the substrate. Field emission scanning electron microscopy (FE-SEM, LEO1530VP and JEOL-JSM 6300), high-resolution transmission electron microscopy (HRTEM; JEM-40001X), Raman spectrometry (J Y HR800), as well as X-ray diffraction (XRD, Philips X′ Pert Pro) were employed to characterize the products. The compositions of the products were analyzed by X-ray photoelectron spectroscopy (XPS, VG ESCALAB MKII) excited by an X-ray source of Mg Kα ($h\nu$ = 1253.6 eV) in an ultrahigh vacuum chamber with a base pressure of $<3 \times 10^{-6}$ Pa. The photoluminescence (PL, Amino Bowman Series-2 spectrometer) emission spectrum was measured at room temperature with a He−Cd laser excitation at 325 nm. Light absorption properties were measured using a UV−vis diffuse reflectance spectrometer (SHIMADZU, UV-2401P) in the wavelength range of 250−800 nm.

Results and Discussion

Figure 1 shows the evolution of the XRD profiles of the products obtained after annealing the $Cu_{0.70}Zn_{0.30}$ brass foil at the marked temperatures in O_2/Ar (O_2, 4%), which indicates that hexagonal wurtzite ZnO (JCPDS card No. 36-1451) is synthesized. SEM and TEM images and corresponding electron diffraction (ED) patterns of the products are shown in Figure 2. Nanosheets with the thickness of 20−100 nm are obtained at reaction temperature (T_R) of 550 °C, while nanocombs with teeth diameter of 20−40 nm are the main product at T_R of 600 °C; the products are mostly composed of nanowires (Figure 2 and Figures S1 and S2 of Supporting Information). This evolution is very similar to our previous study by using $Cu_{0.64}Zn_{0.36}$ as such,[8a] which suggests the faster growth velocity on polar ZnO (0001) surface at higher temperature.[9]

It is noticed that, with an increase in T_R from 550 to 900 °C, the diffraction peaks of Cu−Zn (111), (200) and (220) for Cu−Zn substrate gradually shift to higher diffraction angle and approach the standard XRD pattern for face-centered cubic Cu (JCPDS card No. 03-1005) when T_R > 750 °C (Figure 1). The most obvious shift occurs around 700−750 °C, and similar phenomenon also appears when the oxygen content changes to 2 or 6% O_2 (Figure S1 in Supporting Information). Actually, this phenomenon was observed in our previous study but with a puzzle in our mind at that time.[8a] In the light of Vegard's law,[10] the unit-cell parameter exhibits a linear relationship with Zn content in α-phase brass solid solution. Thus the positions of the diffraction peaks could linearly indicate the Zn content and the sharp peak shift means the sharp decrease of the Zn content within the Cu−Zn substrate. This could be further theoretically understood through a diffusion and sublimation model (Supporting Information). Anyway, more Zn species is

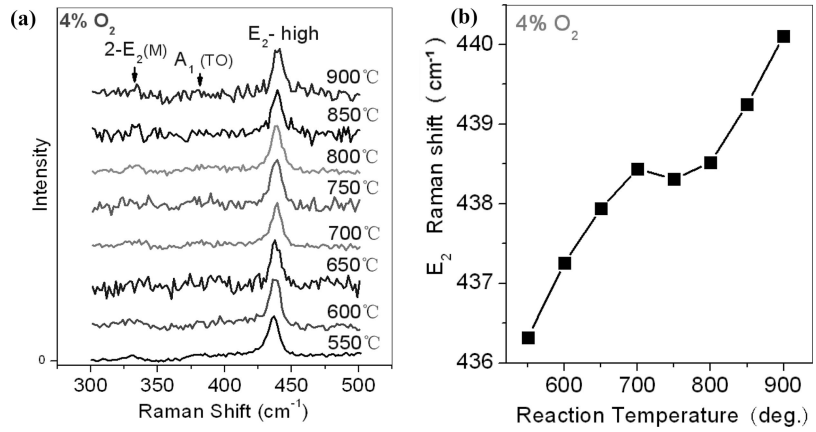

Figure 3. Raman spectra (a) and their E_2 (high) mode shifts (b) of the samples obtained at different T_R. The shifts are obtained by fitting the E_2 mode with Gaussian-type curves.

lost from Cu−Zn alloy at the higher temperature, leading to the faster shift of peaks (111), (200), and (220) to higher diffraction angle. As a result, a sharp shift appears around 700−750 °C as shown in Figure 1. When the Zn species in Cu−Zn alloy is exhausted, XRD pattern correspond to pure Cu would be obtained, which is the cases for the annealing temperature above 750 °C in Figure 1.

To further investigate the structure of the as-synthesized ZnO, micro-Raman spectroscopy is carried out as shown in Figure 3a. The peak at 437 cm^{-1} is attributed to ZnO nonpolar optical phonons high E_2 mode, while the trace peak at 380 cm^{-1} corresponds to the A_1 symmetry with the transverse-optical (TO) mode. The peak at 332 cm^{-1} is assigned to the second-order Raman spectrum arising from Brillouin zone boundary (M point) phonon 2-E_2(M).[1a] It should be noticed that the frequency of the high E_2 mode has a slight blue shift with increase of T_R (Figure 3b) and that the frequency is higher than that for bulk ZnO crystal (437 cm^{-1})[11] when T_R > 600 °C. The E_2 mode is usually used to analyze the stress state in films due to its high sensitivity to stress.[12] Decremps has reported that under pressure, the E_2 (high) frequency of the wurzite ZnO crystal blue-shifted with the increase of biaxial compressive stress within the *c*-axis oriented ZnO epilayers.[13] In Figure 3b, the E_2 (high) frequency of the sample synthesized at higher temperature has larger blue shift, implying larger compressive stress, which may result from more defects such as oxygen vacancy.[14] This case is also observed in the samples obtained by replacing the reaction mixture gas with 4% O_2 by that with 2 or 6% O_2 (Figure S3 in Supporting Information).

XPS analysis is performed to learn the chemical information of the samples. The binding energy is calibrated by taking C1s peak (284.6 eV) as a reference. The surface contamination is removed via Ar^+ bombardment for 0.5 min (ca. 2 nm depletion). For all the samples, the XPS spectra of Zn $2p_{3/2}$ core level have a lonely peak with binding energy of 1021.2 ± 0.2 eV associated with the Zn species in completely oxidized state (Figure 4a).[15] The O1s core level peak has a shoulder at high binding energy side, which could be deconvolved to two subpeaks using Gaussian−Lorentzian curves as shown in Figure 4b. The right component (O1) centered at 530.2 eV is attributed to the O^{2-} ions in the wurzite structure surrounded by Zn atoms with full complement of nearest-neighbor O^{2-} ions, and the left component (O2) at 531.2−531.6 eV to the adsorbed oxygen species and the O^{2-} ions in the oxygen deficient regions.[15,16] The atom ratios of O2/O1 and Zn/O1 have been calculated through the corresponding peak areas together with the sensitivity factors

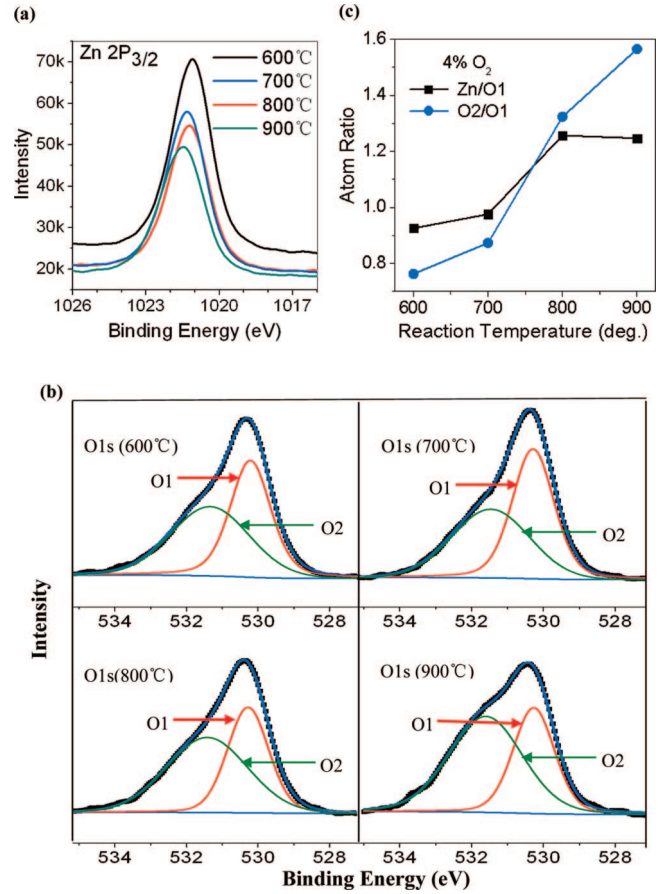

Figure 4. XPS spectra of Zn $2p_{3/2}$ (a) and O1s (b) of the ZnO products synthesized at the marked T_R and the calculated atom ratios of Zn/O1 and O2/O1 vs T_R (c).

(Zn, 4.80; O, 0.66), as displayed in Figure 4c. From the curve of Zn/O1 vs T_R, it is learned that the ZnO_{1-x} products change from around stoichiometric state to oxygen deficiency state with increase of T_R, and the more oxygen deficiency is brought at the higher T_R probably due to the faster growth velocity. Accordingly, O2/O1 should also increase with T_R as shown in the calculated curve of O2/O1 vs T_R in Figure 4c. These results further support the preceding analysis on the Raman characterization. Similar results are also present when changing the oxygen content in the reaction mixture gas (Figure S4 in Supporting Information).

As known, the oxygen vacancy in ZnO will sensitively influence the luminescence properties. Hence this series of

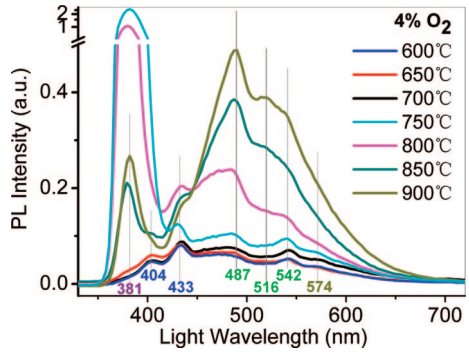

Figure 5. PL spectra of the ZnO products obtained at the marked T_R. Note: The logarithmic scale is adopted for PL intensity larger than 0.5.

ZnO_{1-x} products with different oxygen vacancy (V_O) concentration are further evaluated by room-temperature PL spectra as shown in Figure 5. Generally, the spectra demonstrate strong ultraviolet (UV) emission centered at ~381 nm corresponding to the near band edge (NBE) emission and the visible emission broadband related to intrinsic defects in the ZnO crystal.[6c,7e,17] The blue luminescence at 404 nm could be attributed to zinc vacancy and 433 nm transition to interstitial zinc.[18] The green emissions at 487 and 516 nm are often attributed to oxygen vacancy[1,19] and the 542-nm transition to interstitial oxygen.[18b] The green-yellow emission at 574 nm is also assigned to oxygen vacancy[6c] and interstitial oxygen.[18a] Obviously, the intensity of the green broadband increases with T_R, indicating the increase of V_O concentration. This is in agreement with the results of Raman and XPS characterization. As learned from Figure 1, there is only a slight shift of Cu−Zn diffraction peaks for $T_R \leq$ 700 °C, i.e., only a little Zn species was evaporated and oxidized, hence sparse ZnO nanostructures were produced on the substrate. This should be the main reason for the weak UV peak in Figure 5 for the samples with $T_R \leq$ 700 °C. In the case of $T_R \geq$ 750 °C, the UV peak intensity shows a decreasing tendency with increasing T_R due to the decreasing crystallinity arising from the increasing oxygen defects.

Conclusion

In summary, by simply heating a $Cu_{0.70}Zn_{0.30}$ alloy foil in O_2/Ar, various 1-D ZnO nanostructures have been in situ grown on the conductive metallic substrate. The study on the growth process indicates that more Zn species is lost from Cu−Zn alloy at the higher temperature. Zn species is exhausted, and a sharp diffraction peak shift appears around 750 °C due to the quick depletion. The structures of the ZnO products have been systematically regulated and the more oxygen vacancy is associated with the higher reaction temperature. The correlation in between the oxygen vacancy concentration and the green and exciton emission for these products has been experimentally demonstrated and well understood, which is important for luminescence applications, e.g. to fabricate the ZnO solid state luminescence devices.

Acknowledgment. This work was financially supported by NSFC (20525312), "973" program (2007CB936300), and MOE (No. 208087).

Supporting Information Available: XRD patterns of the ZnO products obtained by changing the oxygen content to 2 and 6% O_2/Ar, typical SEM images of the ZnO products obtained at different T_R with 2, 4, and 6% O_2/Ar, respectively, Raman spectra and the E_2 (high) mode shifts of the ZnO products obtained at different T_R with 2 and 6% O_2/Ar, XPS analysis on the ZnO products synthesized with 4 and 6% O_2/Ar, UV−vis diffuse reflectance spectra of the ZnO products synthesized with 4% O_2/Ar, and explanation about the shifts of Cu−Zn XRD peaks. This information is available free of charge via the Internet at http://pubs.acs.org.

References and Notes

(1) (a) Özgür, Ü.; Alivov, Ya. I.; Liu, C.; Teke, A.; Reshchikov, M. A.; Doğan, S.; Avrutin, V.; Cho, S. J.; Morkoç, H. *J. Appl. Phys.* **2005**, *98*, 041301. (b) Pearton, S. J.; Norton, D. P.; Ip, K.; Heo, Y. W.; Steiner, T. *Prog. Mater. Sci.* **2005**, *50*, 293. (c) Look, D. C. *J. Electron. Mater.* **2006**, *35*, 1299.

(2) Xia, Y. N.; Yang, P. D.; Sun, Y. G.; Wu, Y. Y.; Mayers, B.; Gates, B.; Yin, Y. D.; Kim, F.; Yan, H. Q. *Adv. Mater.* **2003**, *15*, 353.

(3) Huang, M. H.; Mao, S.; Feick, H.; Yan, H. Q.; Wu, Y. Y.; Kind, H.; Weber, E.; Russo, R.; Yang, P. D. *Science* **2001**, *292*, 1897.

(4) (a) Wang, Z. L.; Song, J. H. *Science* **2006**, *312*, 242. (b) Wang, X. D.; Song, J. H.; Liu, J.; Wang, Z. L. *Science* **2007**, *316*, 102. (c) Qin, Y.; Wang, X. D.; Wang, Z. L. *Nature* **2008**, *451*, 809.

(5) (a) Wang, Z. L. *Appl. Phys. A* **2007**, *88*, 7. (b) Zhang, H.; Wu, J. B.; Zhai, C. X.; Du, N.; Ma, X. Y.; Yang, D. R. *Nanotechnology* **2007**, *18*, 455604/1.

(6) (a) Pan, Z. W.; Dai, Z. R.; Wang, Z. L. *Science* **2001**, *291*, 1947. (b) Kong, X. Y.; Ding, Y.; Yang, R. S.; Wang, Z. L. *Science* **2004**, *303*, 1348. (c) Hu, J. W.; Bando, Y. *Appl. Phys. Lett.* **2003**, *82*, 1401. (d) Tang, H.; Chang, J. C.; Shan, Y. Y.; Lee, S. T. *J. Phys. Chem. B* **2008**, *112*, 4016.

(7) (a) Look, D. C.; Claflin, B.; Alivov, Ya. I.; Park, S. *J. Phys. Status Solidi A* **2004**, *201*, 2203. (b) Lu, J. G.; Chang, P. C.; Fan, Z. Y. *Mat. Sci. Eng. R* **2006**, *R52*, 49. (c) Lukas, S. M.; Judith, L. M. D. *Mater. Today* **2007**, *10*, 40. (d) Heo, Y. W.; Norton, D. P.; Tien, L. C.; Kwon, Y.; Kang, B. S.; Ren, F.; Pearton, S. J.; LaRoche, J. R. *Mat. Sci. Eng. R* **2005**, *R47*, 1. (e) Djurišić, A. B.; Leung, Y. H. *Small* **2006**, *2*, 944. (f) Wang, Z. L. *Annu. Rev. Phys. Chem.* **2004**, *55*, 159. (g) Wang, X. D.; Song, J. H.; Wang, Z. L. *J. Mater. Chem.* **2007**, *17*, 711.

(8) (a) Huo, K. F.; Hu, Y. M.; Fu, J. J.; Wang, X. B.; Hu, Z.; Chen, Y. *J. Phys. Chem. C* **2007**, *111*, 5876. (b) Zhu, Y. W.; Sow, C. H.; Yu, T.; Zhao, Q.; Li, P. H.; Shen, Z. X.; Yu, D. P.; Thong, J. T. L. *Adv. Funct. Mater.* **2006**, *16*, 2415. (c) Chen, W. J.; Liu, W. L.; Hsieh, S. H.; Tsai, T. K. *Appl. Surf. Sci.* **2007**, *253*, 6749.

(9) (a) Wang, Z. L.; Kong, X. Y.; Zuo, J. M. *Phys. Rev. Lett.* **2003**, *91*, 185502. (b) Zhang, X. N.; Li, X. R.; Zhang, Z. *Appl. Phys. A* **2006**, *82*, 33.

(10) Vegard, L. *Z. Phys.* **1921**, *5*, 17.

(11) Calleja, J. M.; Cardona, M. *Phys. Rev. B* **1977**, *16*, 3753.

(12) Liao, L.; Lu, H. B.; Li, J. C.; He, H.; Wang, D. F.; Fu, D. J.; Liu, C.; Zhang, W. F. *J. Phys. Chem. C* **2007**, *111*, 1900.

(13) Decremps, F.; Porres, J. P.; Saitta, A. M.; Chervin, J. C.; Polian, A. *Phys. Rev. B* **2002**, *65*, 92101.

(14) Zhang, Y.; Jia, H. B.; Wang, R. M.; Chen, C. P.; Luo, X. P.; Yu, D. P.; Lee, C. *Appl. Phys. Lett.* **2003**, *83*, 4631.

(15) (a) Ramgir, N. S.; Late, D. J.; Bhise, A. B.; More, M. A.; Mulla, I. S.; Joag, D. S.; Vijayamohanan, K. *J. Phys. Chem. B* **2006**, *110*, 18236. (b) Islam, M. N.; Ghosh, T. B.; Chopra, K. L.; Acharya, H. N. *Thin Solid Films* **1996**, *280*, 20. (c) Chen, M.; Wang, X.; Yu, Y. H.; Pei, Z. L.; Bai, X. D.; Sun, C.; Huang, R. F.; Wen, L. S. *Appl. Surf. Sci.* **2000**, *158*, 134. (d) Ye, J. D.; Gu, S. L.; Qin, F.; Zhu, S. M.; Liu, S. M.; Zhou, X.; Liu, W.; Hu, L. Q.; Zhang, R.; Shi, Y.; Zheng, Y. D.; Ye, Y. D. *Appl. Phys. A* **2005**, *81*, 809. (e) De la Rosa, E.; Sepulveda-Guzman, S.; Reeja-Jayan, B.; Torres, A.; Salas, P.; Elizondo, N.; Yacaman, M.; Jose, *J. Phys. Chem. C* **2007**, *111*, 8489.

(16) Coppa, B. J.; Davis, R. F.; Nemanich, R. J. *Appl. Phys. Lett.* **2003**, *82*, 400.

(17) (a) Djurišić, A. B.; Choy, W. C. H.; Roy, V. A. L.; Leung, Y. H.; Kwong, C. Y.; Cheah, K. W.; Gundu, R. T. K.; Chan, W. K.; Lui, H. F.; Surya, C. *Adv. Funct. Mater.* **2004**, *14*, 856. (b) Cui, J. B. *J. Phys. Chem. C* **2008**, *112*, 10385.

(18) (a) Wu, X. L.; Siu, G. G.; Fu, C. L.; Ong, H. C. *Appl. Phys. Lett.* **2001**, *78*, 2285. (b) Lin, B.; Fu, Z.; Jia, Y. *Appl. Phys. Lett.* **2001**, *79*, 943.

(19) (a) Vanheusden, K.; Warren, W. L.; Seager, C. H.; Tallant, D. R.; Voigt, J. A.; Gnade, B. E. *J. Appl. Phys.* **1996**, *79*, 7983. (b) Mahamuni, S.; Borgohain, K.; Bendre, B. S.; Leppert, V. J.; Risbud, S. H. *J. Appl. Phys.* **1999**, *85*, 2861.

JP808679Q